JOURNAL OF THERMOPHYSICS AND HEAT TRANSFER
Vol. 25, No. 1, January–March 2011

Simulation of the Stagnation Region Microcrack Growth During Space Shuttle Reentry

E. V. Titov* and D. A. Levin†
Pennsylvania State University, University Park, Pennsylvania 16802
Brian P. Anderson‡ and Alvaro Rodriguez§
NASA Johnson Space Center, Houston, Texas 77058
and
Donald J. Picetti¶
The Boeing Company, Huntington Beach, California 92647

DOI: 10.2514/1.49993

The newly developed reinforced-carbon–carbon damage assessment model is applied to a micrometeoroid crack at the stagnation point of a sphere for a space shuttle reentry trajectory. The model, which has been validated against arcjet tests (Titov, E., Zhong, J., Levin, D., and Picetti, D., "Simulation of Carbon–Carbon Crack Growth due to Carbon Oxidation in High Temperatures," *Journal of Thermophysics and Heat Transfer*, Vol. 23, No. 3, July–Sept. 2009, pp. 489–501.) (Titov, E., Levin, D., Picetti, D., and Anderson, B. P., "Thermal Protection System Crack Growth Simulation Using Advanced Grid Morphing Techniques," *Journal of Thermophysics and Heat Transfer*, Vol. 24, No. 4, 2010, pp. 708–720.), predicts the microhole wall material response to the high-energy, atomic oxygen rich flow to simulate a micrometeoroid impact of the space shuttle nose cap shield during the STS-5 mission reentry. The extent of the crack damage site hole diameter was found to grow by a factor of 2.7, which agrees within about 30% of the NASA Johnson Space Center reinforced-carbon–carbon damage growth tool, version 2, a semi-empirical approach developed through extensive arcjet testing.

I. Introduction

AN EXTENSION of our modeling of crack damage growth in reinforced-carbon–carbon (RCC) specimens is presented in this work. In our previous work [1,2], we developed a computational technique capable of assessing the extent of RCC damage site growth. The technique was used to estimate the hole growth in a specimen representing a portion of the space shuttle wing [2] and a high-velocity meteoroid impact [3,4] specimen upon exposure to a high-energy, chemically active flow. This approach allowed us to model full three-dimensional crack growth scenarios as well as to include the presence of realistic RCC material features such as delamination, both of which affect damage growth because they enable higher atomic oxygen penetration. The predicted channel growth and shape change were found to agree with arcjet observations and local gas flowfield results. The essence of the developed technique was a wall oxidation model relevant to the conditions in the NASA Johnson Space Center (JSC) arcjet tests of [5] and to the reentry conditions at the altitudes from approximately 90 to 50 km. The computational approach is now being transformed into a computational tool for real time, mission, damage assessment. The purpose of the work presented in this paper is to use the same computational approach and chemical model to predict stagnation site damage growth for a simple geometric sphere flying a space shuttle reentry trajectory.

Received 22 March 2010; revision received 10 September 2010; accepted for publication 7 October 2010.

*Postdoctoral Scholar, Department of Aerospace Engineering. Member AIAA.
†Professor, Department of Aerospace Engineering. Associate Fellow AIAA.
‡Aerospace Engineer, Applied Aeroscience and Computational Fluid Dynamics Branch. Member AIAA.
§Aerospace Engineer, Thermal Design Branch.
¶Associate Technical Fellow, Flight Science and Advanced Design. Member AIAA.

The coupling of gas-dynamic simulations with the thermal protection material response for hypersonic fight is still a challenging problem. Two examples of research related to our work are the modeling of Kuntz et al. [6] and Tang et al. [7]. Coupled computational fluid dynamics (CFD)-RCC material thermal response studies were performed in [6] for a spherical nose cap of a conical reentry vehicle flying a modified IRV-2 trajectory. The modified trajectory increased the heat load to the material, which in turn, resulted in larger wall recession rates. The CFD solution at each trajectory point provided a convective heating rate, recovery enthalpy, and pressure at each surface node, which was loosely coupled to the time-dependent material response simulation. Similar to the work that will be presented here, it was assumed that the CFD steady state aforementioned macroparameters remained constant during the interval between trajectory points. Both the structured CFD and unstructured material computational meshes were periodically adapted as the surface recessed. After 20 s along the reentry trajectory (from ~70 to 0 km), about 1 cm of recession was predicted for the RCC layer in the stagnation region. In the work of Tang et al. [7], the influence of space shuttle orbiter thermal protection system (TPS) damage on the local flowfield was studied. Using CFD they modeled RCC damage cavities in the orbiter heat shield tiles formed because of debris impact and/or missing tiles, and protrusions caused by a dislodged gap filler or RCC repair. The TPS on the vehicle was assumed to be fully catalytic to atom and ion recombination everywhere, and a radiative equilibrium boundary condition with a fixed emissivity was applied everywhere on the surface of the vehicle. The authors used a simplified damage shape to avoid difficulties in the grid generation. The mass loss and shape evolution of the damage site were not modeled as the recession was not expected in the studied areas. The work that we present in this paper considers that influence of the vehicle flowfield on the damage site and uses advanced CFD volume meshing techniques coupled to topology driven material morphing approaches to study the time evolution of a stagnation point microcrack for a hypersonic reentry trajectory.

II. Coupled Trajectory, CFD, and Structural Modeling Approach

The damage is initially modeled as a small, uniform through-hole at the stagnation point of a sphere. The solution proceeds in several

general steps as follows with the shock layer chemistry model presented in Table 1 where standard five component air model was used Starting at an altitude of 80 km, the Navier–Stokes (NS) equations are solved and a wall oxidation model is used to simulate the material response. Typically we choose trajectory points separated by 50–200 s. This means that the damage site wall oxidation rates obtained from the NS solution are treated as constant during that time interval, although, in reality they are changing as the freestream conditions change. During the time between trajectory points, the hole damage surface is morphed using the assumed constant oxidation rate. After the surface morphing is completed [2], a subsequent NS solution is obtained for an updated computational domain and freestream conditions corresponding to the next trajectory point. By starting at 80 and ending at 50 km along the trajectory, we expect to model the bulk of the damage which occurs during the vehicle reentry due to carbon wall oxidation caused by the atomic oxygen produced in the shock layer. The mesh convergence studies were done to make sure that the results are mesh independent. In particular, the solution in the area of the main interest, the channel wall was checked as the mesh density was gradually increased. We first obtained the converged first order accuracy solutions for the solved cases and then applied third order scheme. We did not find differences in the first and third order solutions which guarantees mesh independence.

A. Trajectory Point Selection and Freestream Conditions

The reentry trajectory of the space shuttle studied in this work is taken from [8]. For this trajectory, the altitude rapidly decreases from 120 to 80 km during the first 300 s of the reentry and then continues to decrease at a lower rate after the vehicle enters the higher density layers of the Earth's atmosphere to begin lifted flight. The velocity of the vehicle does not change much during the first 310 s of the flight and the vehicle enters the higher density layers at a speed of around 7.5 km/s. We therefore start our modeling at 80 km (310 s into the reentry trajectory) and continue down to an altitude sufficiently low such that the carbon oxidation rate is again insignificant because the freestream Mach number is too low to produce sufficient atomic oxygen in the shock layer. We assume the wall temperature to be 1831 K throughout the modeling, which corresponds to the temperature flight data presented Fig. 22 of [9]. Although the wall temperature was obtained for the wing leading edge, we assume it to be similar to that of the space shuttle nose cap area, which is the emphasis of our modeling, since both of these surfaces are subjected to flow conditions similar to the stagnation regime. The flow conditions at different altitudes were obtained from the MSIS Earth atmosphere model and are presented in Table 2. For this altitude range the freestream mass fractions of molecular nitrogen and molecular oxygen remain relatively constant and were assumed to be 0.77 and 0.23, respectively.

B. Computational Flow and Wall Recession Models and Morphing

The computational domain, shown in Fig. 1, encompasses a sphere of a radius of 0.718 m. The extent of the computational domain was such that it allowed the shock wave in front of the sphere to be captured and included the subsonic wake region behind the sphere. The wake flow beyond a Mach number of unity was excluded from consideration since it has no influence on the flow in the vicinity of the damage site (the major interest in this study). A hole with an initial

Table 1 Arrhennius parameters of chemical reactions

	Forward rates[a]			Equilibrium rates[b]		
Reaction	C	ν	$-\varepsilon/kT$	C	ν	$-\varepsilon/kT$
$N_2 + N_2 \rightarrow N + N + N_2$	4.7×10^{14}	−0.5	113,000	18,000	0	113,000
$N_2 + O_2 \rightarrow N + N + O_2$	1.9×10^{14}	−0.5	113,000	18,000	0	113,000
$N_2 + NO \rightarrow N + N + NO$	1.9×10^{14}	−0.5	113,000	18,000	0	113,000
$N_2 + N \rightarrow N + N + N$	4.085×10^{19}	−1.5	113,000	18,000	0	113,000
$N_2 + O \rightarrow N + N + O$	1.9×10^{14}	−0.5	113,000	18,000	0	113,000
$O_2 + N_2 \rightarrow O + O + N_2$	7.2×10^{15}	−1	59,500	1,200,000	−0.5	59,500
$O_2 + O_2 \rightarrow O + O + O_2$	3.24×10^{15}	−1	59,500	1,200,000	−0.5	59,500
$O_2 + NO \rightarrow O + O + NO$	3.6×10^{15}	−1	59,500	1,200,000	−0.5	59,500
$O_2 + N \rightarrow O + O + N$	3.6×10^{15}	−1	59,500	1,200,000	−0.5	59,500
$O_2 + O \rightarrow O + O + O$	9.0×10^{16}	−1	59,500	1,200,000	−0.5	59,500
$NO + N_2 \rightarrow N + O + N_2$	3.9×10^{17}	−1.5	75,500	4000	0	75,500
$NO + O_2 \rightarrow N + O + O_2$	3.9×10^{17}	−1.5	75,500	4000	0	75,500
$NO + NO \rightarrow N + O + NO$	7.8×10^{17}	−1.5	75,500	4000	0	75,500
$NO + N \rightarrow N + O + N$	7.8×10^{17}	−1.5	75,500	4000	0	75,500
$NO + O \rightarrow N + O + O$	7.8×10^{17}	−1.5	75,500	4000	0	75,500
$O + N_2 \rightarrow N + NO$	$7.0 \times 10^{1}0$	0	38,000	4.5	0	37,500
$NO + O \rightarrow N + O_2$	3, 200, 000	1	19700	0.00333	0.5	16,000

[a]Presented are the coefficients in the formula $K_f = CT_a^{\eta} e^{-\varepsilon/kT}$, where k is Boltzmann constant, T_a is the rate controlling temperature defined as $T_a = T^{\alpha} T_v^{\beta} T_e^{1-\alpha-\beta}$, T_v is vibrational temperature, and T_e is electron temperature. In the solved cases, $\alpha = 1$, $\beta = 0$.
[b]Presented are the coefficients in the formula $K_c = CT^{\eta} e^{-\varepsilon/kT}$: ε/kT is activation energy.

Table 2 Freestream conditions for trajectory points taken from the STS-5 reentry trajectory[a]

Altitude, km	Time[b], s	N_2, $1/cm^3$	O_2, $1/cm^3$	Mass density g/cm^3	T, K	Velocity, km/s
80	310	$2.281 \times 10^{+14}$	$6.071 \times 10^{+13}$	1.400×10^{-8}	213.7	7.75
77.5	400	$3.265 \times 10^{+14}$	$8.711 \times 10^{+13}$	2.006×10^{-8}	219.3	7.5
75.0	575	$4.660 \times 10^{+14}$	$1.245 \times 10^{+14}$	2.864×10^{-8}	223.9	7.1
70.0	800	$9.524 \times 10^{+14}$	$2.549 \times 10^{+14}$	5.856×10^{-8}	228.7	6.2
60.0	1000	$3.787 \times 10^{+15}$	$1.016 \times 10^{+15}$	2.330×10^{-7}	240.6	5.05
50.0	1160	$1.361 \times 10^{+16}$	$3.651 \times 10^{+15}$	8.373×10^{-7}	257.9	3.6
47.5	1260	$1.863 \times 10^{+16}$	$4.999 \times 10^{+15}$	1.146×10^{-6}	260.6	2.75
40.0	1360	$5.161 \times 10^{+16}$	$1.384 \times 10^{+16}$	3.175×10^{-6}	250.7	2.00

[a]Freestream conditions come from the MSIS data base.
[b]Times indicate points taken from the STS-5 trajectory.

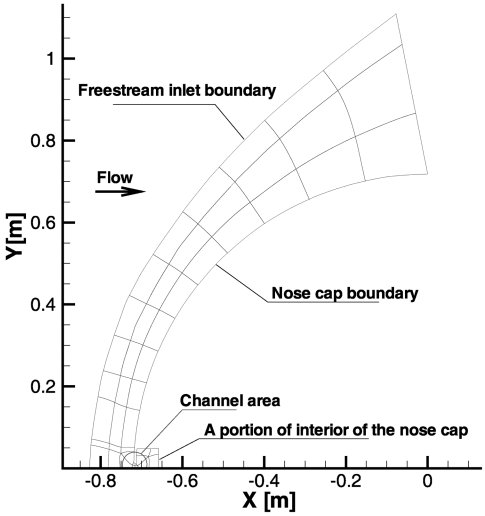

Fig. 1 Computational domain.

diameter of 14.8 and depth of 5.9 mm corresponding to a sample hypervelocity impact damage was located at the stagnation point of the sphere. The multiblock structure of the axisymmetric computational domain is shown in Fig. 1. There were 34 mesh blocks in the freestream, four blocks inside the channel and four blocks in the interior portion of the vehicle nose. The shapes of the blocks in the vicinity of the channel and within the interior zone were adapted to construct a mesh of good quality with respect to the cell orthogonality and stretching ratio. The mesh points were clustered at the channel wall and in the shock wave region. The entire mesh consisted of 37,225 cells for the 1000 s (60 km) case and was decomposed into 76 partitions. Solution convergence required 6–8 h runs on 40 1.5 GHz processors which ensured a drop of the residuals of 7–8 orders of magnitude compared with the initial value. The mesh convergence was guaranteed by sequencing the solution into several runs with increasing mesh density and increasing computational scheme accuracy (such an option is available in the GASP [10]) computational tool. The observed difference between the solutions obtained with the highest mesh density and with the second to the highest mesh density was negligible. This guaranteed the mesh independence of the obtained solution.

The numerical solutions of the NS equations for viscous, chemically reacting flow were obtained using the GASP commercial software [10]. Since the flow regime was continuum with respect to the vehicle nose radius for the trajectory point cases modeled, the no-slip boundary conditions were used. The chemical reactions of the six chemical species of N_2, O_2, N, O, NO, and CO were modeled in the entire computational domain using the chemical reactions and rates given in [11]. Chemical reactions were found to be important in the shocklayer region, but, not in the internal damage site cavity flow, as consistent with previous work [1]. The CO species is formed in the carbon oxidation of the wall as discussed next.

The RCC thermal protection material is composed of graphite fibers embedded in a carbon matrix coated with a layer of silicon carbide (SiC) that protects the bare carbon from oxidation [12]. Unlike other studies that have been concerned with understanding the robustness of the silica layer, our starting conditions are based on the assumption that a known region of the protective SiC layer has been removed as a result of impact and that only bare carbon is exposed [1,2]. As is discussed in [5], atomic oxygen plays an important role in carbon mass surface loss. For the conditions of Shuttle reentry an important mechanism for removal of atomic carbon is

$$C_{(s)} + O \rightarrow CO \tag{1}$$

where $C_{(s)}$ is a carbon atom at the wall surface and the other species are gaseous. Reference [13] gives a probability close to 0.9 for this gas surface reaction, for a gas temperature of about 1500 K, $C_{(s)}$. This

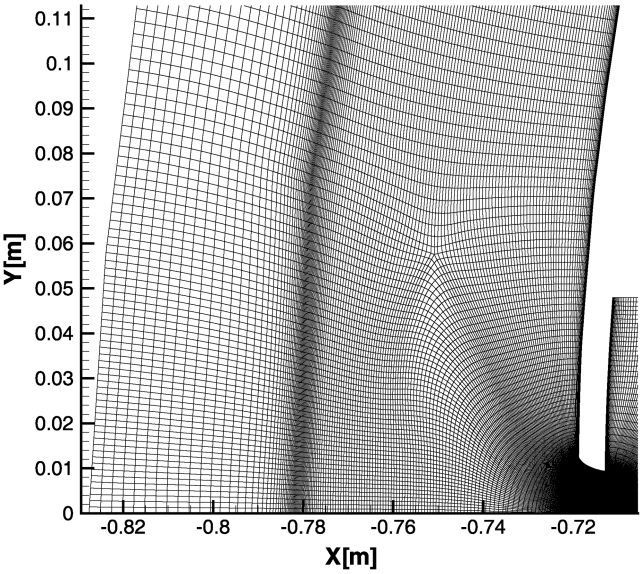

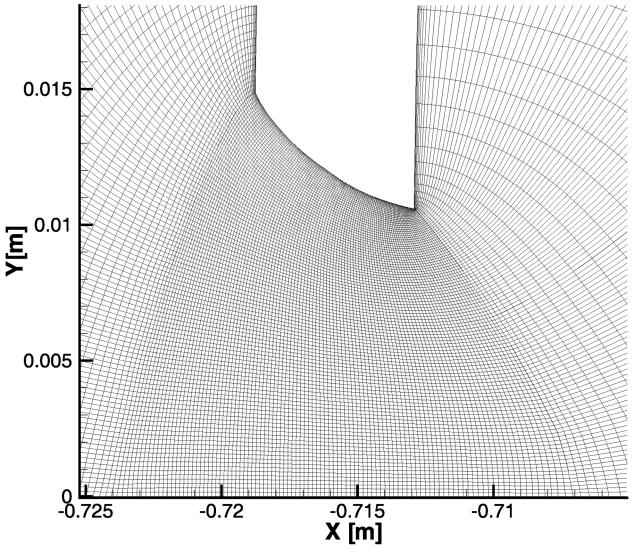

Fig. 2 Portions of the mesh for Case 1000 s (60 km). The top and bottom figures show the shock wave captured in the stagnation portion of the flow and an enlargement of a morphed channel area, respectively.

reacting wall boundary condition was implemented in the GASP [10] commercial CFD software.

We start the damage site growth modeling off by obtaining the CFD solution at 80 km, using it to calculate the surface recession at each location inside the damage site, and then morphing the exposed surface using the GridPro [14] topology-based procedures developed in our earlier work [2]. After the surface is morphed a new volume mesh is generated within Gridpro for use in the next CFD calculation at w new trajectory point. Figure 2 shows portions of the computational mesh for one of the iterations corresponding to the 1000 s (60 km) case. The top portion of the figure presents the mesh in the stagnation region of the flow. The figure demonstrates the shock wave capturing meshing feature, which, is important in this study since the dissociation of molecular oxygen in the shock layer is the only source of the atomic oxygen, the component which causes the damage site wall recession. The bottom portion of the figure presents the mesh inside the channel. The accumulated recession along the channel wall to this point in the reentry is represented by its deviation from the initial uniform hole radius of 0.0075 m. The corresponding volume grid generated by the morphing procedure includes mesh points clustered in the boundary layer region of the flow (close to the channel wall) to resolve the gradients in an area of the primary interest of this study. Since the topology of the computational domain does not change throughout the trajectory, the meshing of previous

and subsequent cases was easily performed after the initial topology was build using the techniques available in GridPro [2,14]. Creating high-quality meshes that capture the external and internal flow gradients was relatively straightforward for the solved axisymmetric cases.

III. Results and Discussion

The first calculation was performed for the 80 km conditions (310 s) using the reentry trajectory discussed preceding. The next calculation was done at 400 s where it was found that the oxidation rate increased, but, not significantly. For this reason the subsequent computations were performed with larger time intervals corresponding to times of 575, 800, 1000 and 1160 s and the total time interval modeled corresponds to a range of altitudes from 80 to 50 km. We start the presentation of results with a comparison of the flow properties in the shock layer in front of the sphere for the two altitudes of 80 km (310 s) and 60 km (1000 s). As can be seen in Fig. 3, the major flow parameters change with the maximum flow temperature in the shock layer declining and the stagnation density rising as the vehicle descends into the higher density layers of the atmosphere and decelerates. It can also be seen that although the shock layer becomes narrower, the shock stand off distance decreases and the shock layer temperatures decline compared with the initial values at 80 km. The temperature and the gas flow residence time in the shock layer region is still sufficient for the entire amount of the molecular oxygen to dissociate which results in an almost constant mass fraction of atomic oxygen behind the shock wave. It should be noted, however, that the thermochemical model used here assumes that the molecular oxygen dissociation rate depends only on the translational temperature. A more accurate representation, *e.g.*, based on the Park $\sqrt{TT_v}$ model would probably show the degree of dissociation is overestimated.

Figures 4 and 5 compare the flow quantities inside the damage site channel at two points along the trajectory. It can be seen in Fig. 4 that the flow density at the wall of the channel increases significantly in the 1000 s case while the flow temperature near the wall does not change much. The mass fraction of the atomic oxygen near the wall, however, does change at 1000 s decreasing substantially as compared with the first reentry point of 310 s (see Fig. 5). This is probably due to changes of the channel shape with the channel wall being more exposed to the flow at 1000 s due to the already recessed surface *i.e.*, the channel has opened up more. The increase of the CO mass fraction in front of the channel wall is also greater in the 1000 s case, reflecting higher oxidation rate, but the presence of larger quantities of CO also shields the surface from the incoming atomic oxygen and therefore preventing further oxidation.

To check the influence of wall temperature on the atomic oxygen production in the shock layer a calculation was performed at an altitude of 70 km (575 s) with a lower wall temperature of 300 K. The top portion of the Fig. 6 presents the flow temperature along the stagnation line for two wall temperatures of 1831 and 300 K and the bottom portion presents the mass fraction of atomic oxygen along the stagnation line. As can be seen in the figure the stand off distance

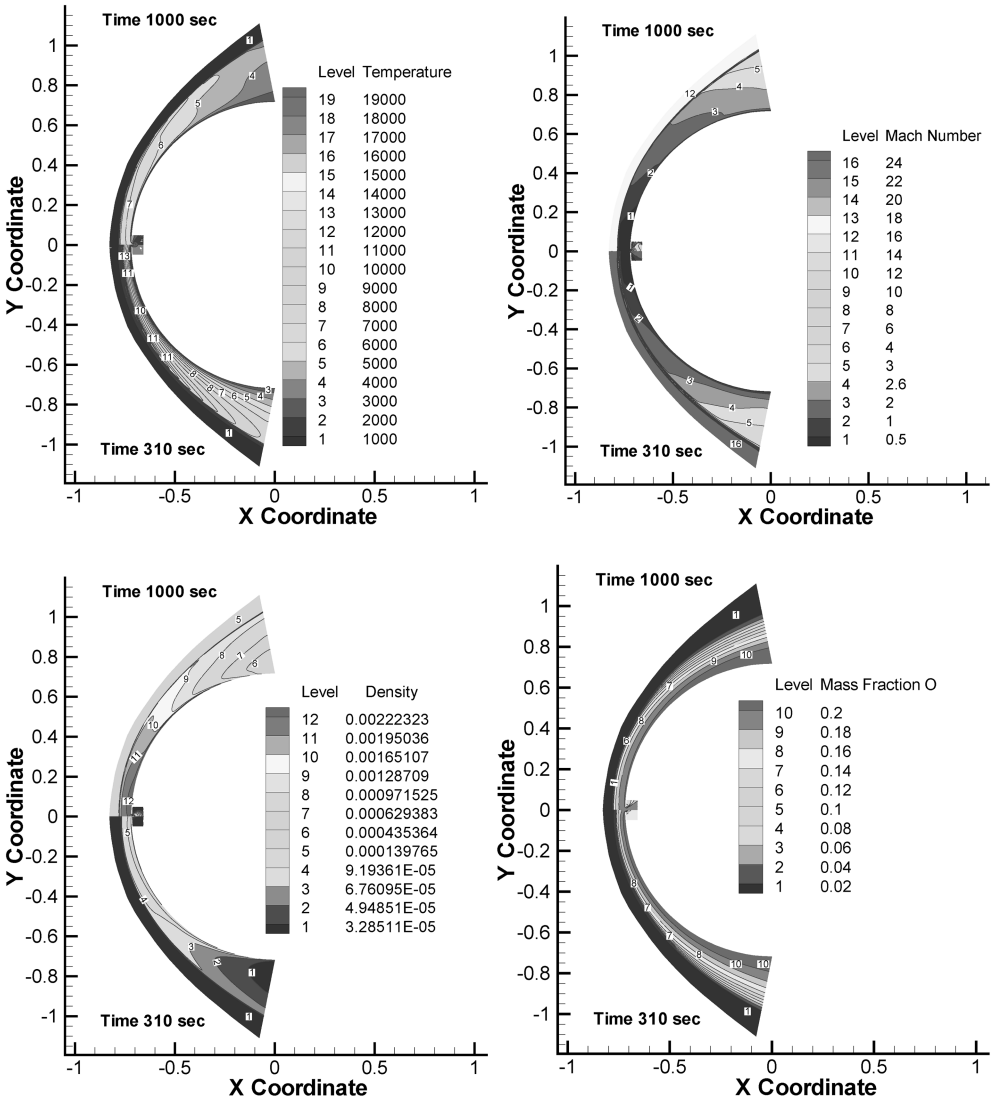

Fig. 3 Flow parameters at 310 and 1000 s. Temperature is in K and the flow density is in $\mathrm{kg/m^3}$. Coordinates are in meters.

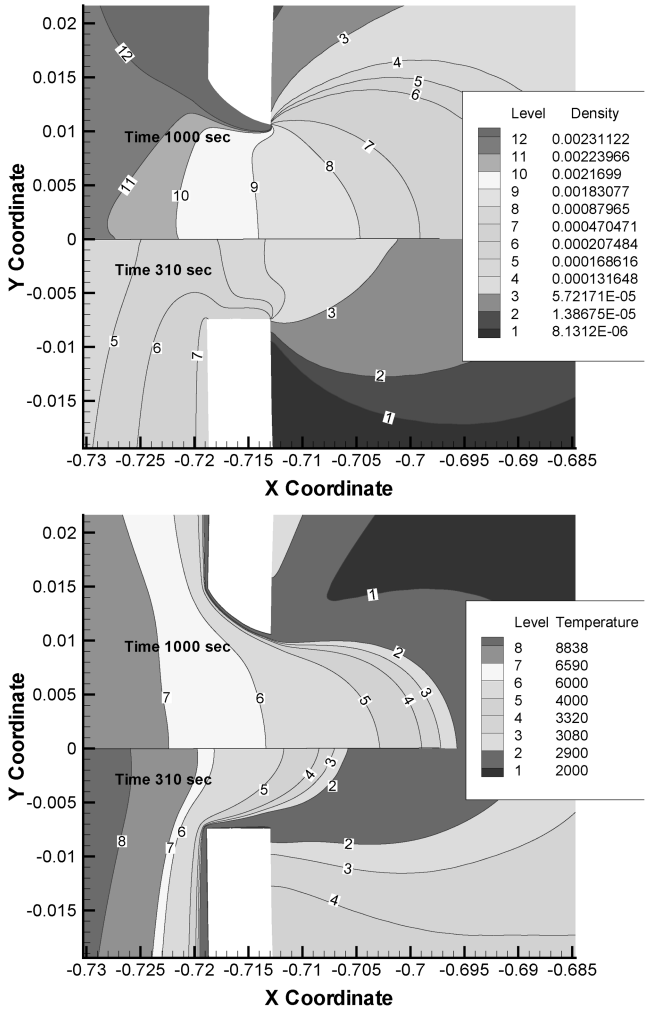

Fig. 4 Flow parameters in the channel at 310 and 1000 s. Top: density (kg/m^3). Bottom: temperature (K). Coordinates are in meters.

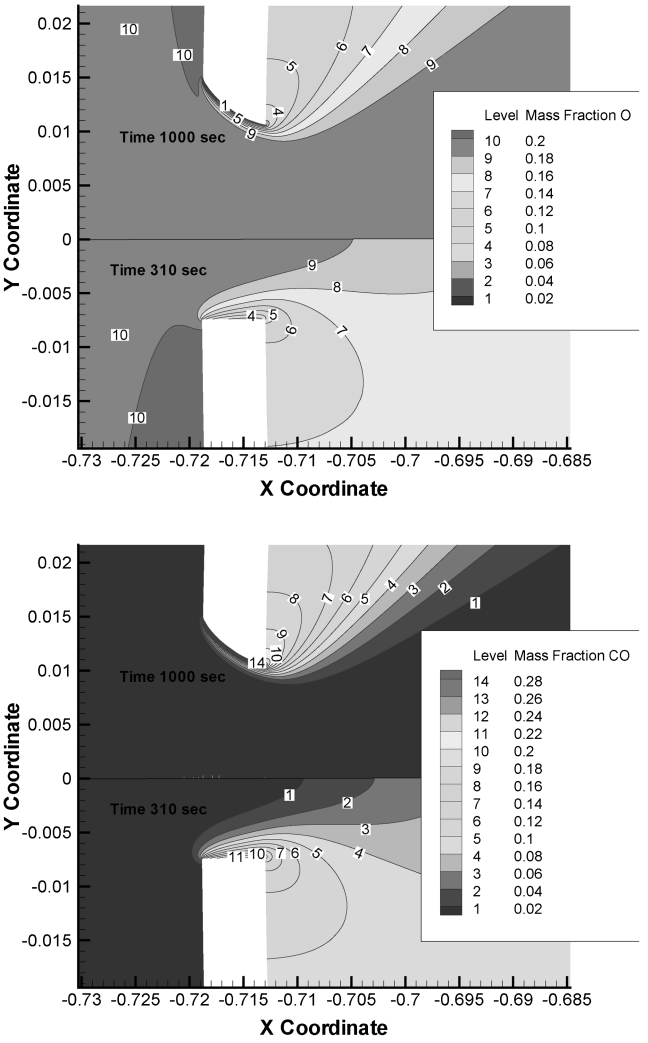

Fig. 5 Flow parameters in the channel. Top: O mass fraction. Bottom: CO mass fraction. Coordinates are in meters.

of the shock wave significantly changes, decreasing as the wall temperature decreases, but, the value of the temperature rise and the amount of the atomic oxygen behind the shock do not change. This result suggests that the wall temperature is not a large factor in the present study and the initial assumption of a constant wall temperature of 1831 K for the entire portion of the trajectory under consideration is satisfactory.

The major result of this study is illustrated in the top portion of Fig. 7 where the oxidation rate is presented along the channel wall for the time interval corresponding to the most active oxidation. Figure 7 also presents the channel wall shape at different times illustrating the wall recession progress. As can be seen in the figure the oxidation rate increases by a factor of 8 during the descent from 80 to 60 km and then decreases at an altitude of 50 km. The oxidation rate decreases further as computed at the three following time stations (not presented in the figure) reaching an insignificant value of the order of 1.0×10^{-9} at an altitude of 40 km. Several factors influence the rate including the flow density and velocity as well as channel shape. As the vehicle descends the flow mass density rises but the flow velocity drops which results in an initial increase of the oxidation rate due to the increasing atomic oxygen density in the flow. Later in the trajectory, when the vehicle decelerates significantly, the atomic oxygen production drops and the rate decreases at an altitude of around 50 km. The channel shape change additionally complicates the relationship between the vehicle trajectory and the wall oxidation rate because as the channel surface becomes more and more exposed to the incoming flow, the surface recesses faster as the oxidation rates increase at the channel entrance. It was found that the oxidation rate peaks at around 60 km which also corresponds to the point of the maximum heating according to [9].

The channel wall shapes at different times are presented in the bottom portion of Fig. 7. After the first iteration, the channel shape change is not uniform with the maximum change observed at the entrance of the channel. As the altitude decreases, the channel recession rate downstream of the entrance decreases faster because the available atomic oxygen is consumed by the chemically active wall. The total hole growth at the entrance of the channel at 40 km is a factor of 3.0 greater than the original hole diameter. This level of hole growth accounts for the major portion of the material loss since the most chemically active portion of the trajectory has been completed at this point.

The damage site diameter growth dynamics predicted by the presented computations agrees well during the first 1100 s of the trajectory with the estimations of the JSC RCC damage growth tool, version 2, a semi-empirical approach developed through extensive arcjet testing 15. A comparison of the hole damage site sizes predicted by the two techniques is presented in Fig. 8. The values presented in Fig. 8 are the average of Fig. 7, computed based on the results of this work, since the JSC RCC damage growth tool does not predict the hole profile but instead gives an average whole diameter. The CFD based analysis predicts the oxidation process to continue beyond a time of around 1100 s whereas the NASA damage growth tool predicts the hole growth to stop. Also it can be seen in Fig. 8 that if the computational results are shifted to earlier times better agreement between the two curves would be obtained. We assumed that oxidation rate would be small before 80 km, in contrast to the JSC tool. The hole growth predicted by the CFD technique levels off at around 1300 s resulting in an over estimation of the hole size of about 30% as compared with the semi-analytical tool.

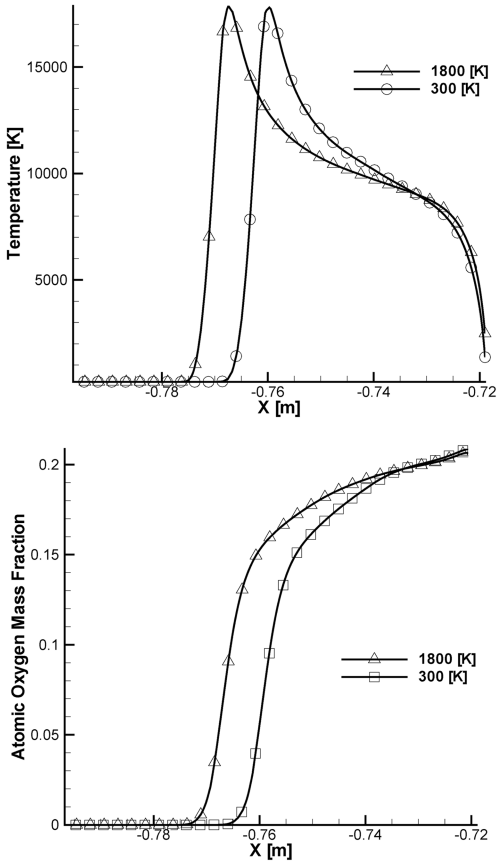

Fig. 6 Flow parameters along the stagnation line at 575 s for two wall temperatures. Top: flow temperature (K). Bottom: O mass fraction. Coordinates are in meters.

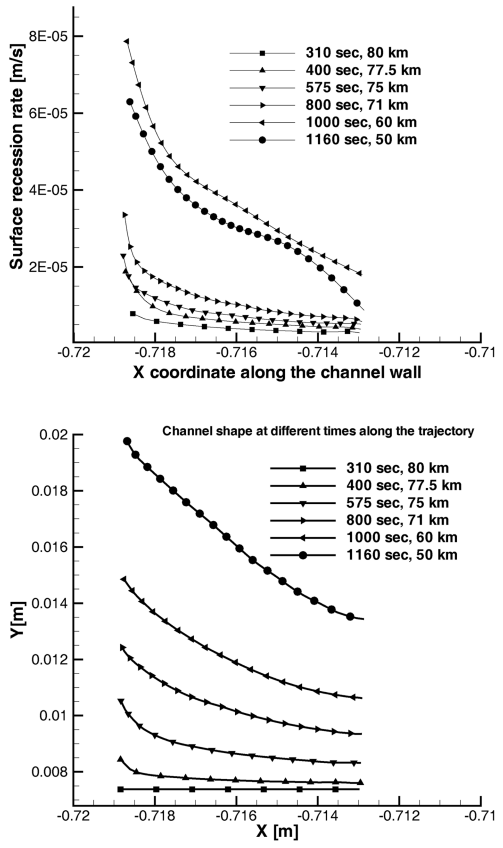

Fig. 7 Top: channel wall oxidation rates at different times. Bottom: channel shape at different times. Coordinates are in meters.

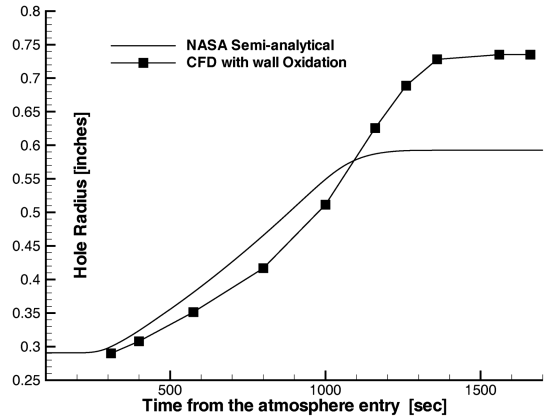

Fig. 8 Comparison of the hole growth predicted by the semi-analytical JSC RCC damage growth tool and the presented CFD approach.

The discrepancies between the two results may be due to three factors: (1) neglect of local effects in the damage site area, (2) frequency of trajectory points included in the iteration procedure, and (3) overestimate of the molecular oxygen dissociation rate by the applied finite rate chemical model. However, despite the discrepancy, the CFD approach captures the physics of the problem correctly and the agreement between the two results is encouraging, particularly because the approach presented here can be generalized to reentry scenarios where the mass loss regression rate correlations have not been established.

IV. Conclusions

An analysis of the damage site growth in RCC due to carbon oxidation at the stagnation point of a sphere was made for the space shuttle STS-5 reentry trajectory. Our previously developed techniques were used to mesh the changing computational domain and to adapt the mesh to the flow parameters at different altitudes. The influence of the surface temperature on the production of the atomic oxygen in the flow and the flow parameters in general was also studied. We found that the production of atomic oxygen due to molecular oxygen dissociation in the shock layer at high temperatures removed sufficient amounts of wall carbon for a circular damage site to grow. We also found that the maximum wall oxidation occurs at around 60 km due to the combination of increasing flow density and sufficiently high vehicle velocity which results in the significant production of atomic oxygen in the shock layer. As the velocity decreased further into the reentry trajectory, the oxidation rate was also found to decrease. The modeling encompassed the trajectory points from 80 to 50 km thereby assuming that the bulk of the surface recession process has been captured. We found that the damage site hole diameter grew by a factor of 2.7 from a diameter of 14.8 to 40 mm, putting us within reasonable agreement of the present semi-empirical mass loss regression approaches.

Acknowledgments

E. V. Titov and D. A. Levin would like to acknowledge support from NASA Grant NNX08AD84G from NASA/Johnson Space Flight Center. We would especially like to thank the AeroSoft Corporation, Blacksburg, Virginia, for their technical support and assistance in incorporating the gas wall oxidation boundary condition.

References

[1] Titov, E., Zhong, J., Levin, D., and Picetti, D., "Simulation of Carbon–Carbon Crack Growth due to Carbon Oxidation in High Temperatures ," *Journal of Thermophysics and Heat Transfer*, Vol. 3, No. 3, July–Sept. 2009, pp. 489–501.

[2] Titov, E., Levin, D., Picetti, D., and Anderson, B. P., "Thermal Protection System Crack Growth Simulation Using Advanced Grid Morphing Techniques," *Journal of Thermophysics and Heat Transfer*,

Vol. 24, No. 4, 2010, pp. 708–720.
doi:10.2514/1.48046

[3] Curry, D. M., Pham, V. T., Norman, I., and Chao, D. C., "Oxidation of Reinforced Carbon–Carbon Subjected to Hypervelocity Impact," NASA TP-2000-209760, March 2000.

[4] Curry, D., Pham, V., Norman, I., and Chao, D., "Oxidation of the Reinforced Carbon–Carbon Subjected to Hypervelocity Impact," NASA TP 2000-209760, March 2000.

[5] Curry, D., Johansen, K., and Stephens, E., "Reinforced Carbon-Carbon Oxidation Behavior in Convective and Radiative Environments," NASA TP 1284, 1978.

[6] Kuntz, D. W., Hassan, B., and Potter, D. L., "Predictions of Ablating Hypersonic Vehicles Using an Iterative Coupled Fluid/Thermal Approach," *Journal of Thermophysics and Heat Transfer*, Vol. 15, No. 2, 2001, pp. 129–139.

[7] Tang, C., Saunders, D., Trumble, K., and Driver, D., "Rapid Aerothermal Simulations of Damage and Repair During a Space Shuttle Mission," AIAA Paper No. 2007-1783, April 2007.

[8] Gong, L., Ko, W. L., and Quinn, R. D., "Thermal Response of Space Shuttle Wing During Reentry Heating," NASA TM 85907, June 1984.

[9] Curry, D. M., Pham, V. T., Norman, I., and Chao, D. C., "Oxidation of Reinforced Carbon–Carbon Subjected to Hypervelocity Impact," NASA TP-2000-209760, March 2000.

[10] Gasp, The General Aerodynamic Simulation Program, Computational Flow Analysis Software for the Scientist and Engineer, User's Manual, Aerosoft Co., Blacksburg, VA, 1996.

[11] Titov, E., Levin, D., Picetti, D., and Anderson, B. P., "Simulation of TPS Crack Growth due to Carbon Oxidation Using Advanced Grid Morphing Techniques," AIAA Paper 2009-3599, 41st AIAA Thermophysics Conference, San Antonio, TX, 22–25 June 2009.

[12] Jacobson, N., Leonhardt, T., Curry, D., and Rapp, R., "Oxidative Attack of Carbon/Carbon Substrates Through Coating Pinholes," *Carbon*, Vol. 37, No. 3, 1999, pp. 411–419.
doi:10.1016/S0008-6223(98)00206-1

[13] Rosner, D., and Allendorf, H. D., "High-Temperature Kinetics of Graphite Oxidation by Dissociated Oxygen," *AIAA Journal*, Vol. 3, Aug. 1965, pp. 1522–1523.
doi:10.2514/3.3186

[14] Eiseman, P. R., "Adaptive Grid Generation," *Computer Methods in Applied Mechanics and Engineering*, Vol. 64, Nos. 1–3, March 1987, pp. 321–376.
doi:10.1016/0045-7825(87)90046-6